COMMUNICATION

Excitation and Valence Induced Photoluminescence Control in Bi-Eu Activated Double Perovskite Phosphor for Future Intelligent LEDs Lighting

Yi Wei, Hang Yang, Zhiyu Gao, Gongcheng Xing, Maxim S. Molokeev, Guogang Li*

Abstract: Intelligent light emitting diodes (LEDs) lighting attracts much attention in indoor lighting sources. However, the development of phosphors with wide photoluminescence tuning is crucial. Herein, a novel Bi^{3+}-doped $La_2Mg_{1.14}Zr_{0.86}O_6$ double perovskite phosphor with excitation-induced blue/green photoluminescence tuning is reported. The corresponding mechanism is mainly caused by the coexistence of Bi^{2+} and Bi^{3+} ions based on a native oxygen vacancy. By simultaneously designing $Bi^{3+} \rightarrow Eu^{3+}$ energy transfer, single-composition white light with wide-range adjustable corrected color temperatures (CCT) is successfully achieved by controlling excitation wavelength and Eu^{3+} concentration. This method initiates a new insight to explore phosphors with excitation-induced photoluminescence tuning and wide CCT control for future intelligent LEDs lighting.

Recently, with the rapid development of artificial intelligence industry, intelligent light emitting diodes (LEDs) technique gradually becomes a popular trend in solid state lighting field [1-2]. The goal of intelligent LEDs lighting is to achieve intelligent control of lighting equipment. It involves the functions of free luminescence adjustment, light soft start, timing control, scene setting and so on [3]. This intelligent LEDs technique has many advantages, such as safety, energy saving, comfort and high efficiency [4-6]. As the indispensable component of LEDs devices, the phosphors with adjustable photoluminescence are highly desired in intelligent LEDs lighting. Up to now, many strategies have been reported to achieve photoluminescence adjustment for phosphors, such as phase transition [7-9], component substitution [10-11] and energy transfer strategies[12-13]. Phase transition can efficiently change the local lattice structure. For instance, Zhao et al. reported a photoluminescence-adjustable $NaAlSiO_4:Eu^{2+}$ phosphor, which produces blue (460 nm) and yellow light (540 nm) in low-carnegieite ($P3_2$) and nepheline phases ($P6_3$), respectively [14]. However, it needs to change experimental condition, so phase transition induced photoluminescence adjustment can't well meet the requirement of intelligent LEDs. Component substitution strategies include cation substitution, anion substitution, and cation-anion substitution, these strategies mainly modulate the local coordination environment around activator ions [15-18]. For example, $(Y,Sc)(Nb,V)O_4:Bi^{3+}$ phosphors can successfully achieve large-scale photoluminescence adjustment from blue (450 nm) to red light (647 nm) by continuous component substitution [19]. However, component substitution strategies are hard to generate single-composition white light emission. Designing energy transfer including $Ce^{3+}\rightarrow Eu^{2+}$, $Eu^{2+}\rightarrow Mn^{2+}$, $Ce^{3+}\rightarrow Tb^{3+}$, $Eu^{2+}\rightarrow Tb^{3+}$, $Bi^{3+}\rightarrow Eu^{3+}$, $Bi^{3+}\rightarrow Mn^{4+}$ can achieve full-spectrum photoluminescence tuning over the whole visible area [20]. Nevertheless, the energy transfer efficiency is relatively low, and the photoluminescence intensity needs to be further optimized. As a consequence, the development of phosphors with full-spectrum photoluminescence adjustment is still a crucial challenge.

As previously reported, an photoluminescence emission (PL) redshift might occur with increasing excitation wavelength in some carbon nanostructures, and more significantly, the emission can almost cover the entire visible range [21]. Such an excitation-induced photoluminescence tuning can well meet the requirement of intelligent LEDs because the luminescence performance can be tuned by just changing the LED chips. For rare earth ions (Eu^{2+}, Ce^{3+}) and Bi^{3+} ions activated multiple-cation-sites phosphors, excitation wavelength may also induce a photoluminescence tuning since those activators are sensitive to the surrounding coordination environment [16, 22]. However, the shift in emission peak is not large, and thus, the excitation-induced photoluminescence tuning is hard to cover full-spectrum range. Besides, this excitation-induced photoluminescence tuning is seldom reported in the phosphor matrix that contains only one luminescence center, and the corresponding mechanism is unclear. Hence, exploiting novel phosphors with excitation-induced photoluminescence tuning is still a crucial challenge in the development of intelligent LEDs.

In this work, we focus on the photoluminescence tuning performance of Bi^{3+} ions. Compared to rare earth ions, Bi^{3+} ions have many advantages such as environment friendly, abundant storage and cheap [23]. Furthermore, the absorption region mainly locates in the near-ultraviolet (n-UV) region, largely avoiding spectral overlap and enhancing the luminescence efficiency [24]. More importantly, Bi^{3+} can emit various light from violet to near-infrared color by modulating the local coordination structure [25-26]. Herein, when Bi^{3+} ions are doped in $La_2Mg_{1.14}Zr_{0.86}O_6$ double perovskite phosphors, a novel excitation-induced photoluminescence adjustment is successfully achieved from blue to green light. The X-ray photoelectron spectroscopy (XPS) results confirm the co-existence of Bi^{3+} and

[a] Dr. Y. Wei, Dr. H. Yang, Dr. Z. Gao, Dr. G. Xing, Prof. G. Li
Engineering Research Center of Nano-Geomaterials of Ministry of Education, Faculty of Materials Science and Chemistry,
China University of Geosciences
Wuhan, Hubei, 430074, P. R. China
E-mail: ggli@cug.edu.cn
[b] Prof. Dr. M. S. Molokeev
Laboratory of Crystal Physics, Kirensky Institute of Physics
Federal Research Center KSC SB RAS
Krasnoyarsk 660036 (Russia)
and
Siberian Federal University
Krasnoyarsk 660041 (Russia)
and
Department of Physics, Far Eastern State Transport University
Khabarovsk, 680021 (Russia)

Supporting information for this article is given via a link at the end of the document.

Bi^{2+} ions. Due to only one Bi^{3+} luminescence center, the successive excitation-induced PL redshift is attributed to the co-existence of Bi^{2+} and Bi^{3+}. Then the $Bi^{3+}\rightarrow Eu^{3+}$ energy transfer is designed. Under a varied excitation wavelength (300-370 nm), the photoluminescence color is tuned in the full-spectrum range, and thus a wide white light emission with different CCT across cold white to warm white region is achieved. Based on the above results, a conceptual device is designed through $La_2Mg_{1.14}Zr_{0.86}O_6$:0.07$Bi^{3+}$, *y*$Eu^{3+}$, which can be applied in the future intelligent LEDs lighting. This phenomenon offers an initial guidance to design excitation-induced-photoluminescence-adjustable phosphors for the full-spectrum LEDs lighting with variable CCT and emission color.

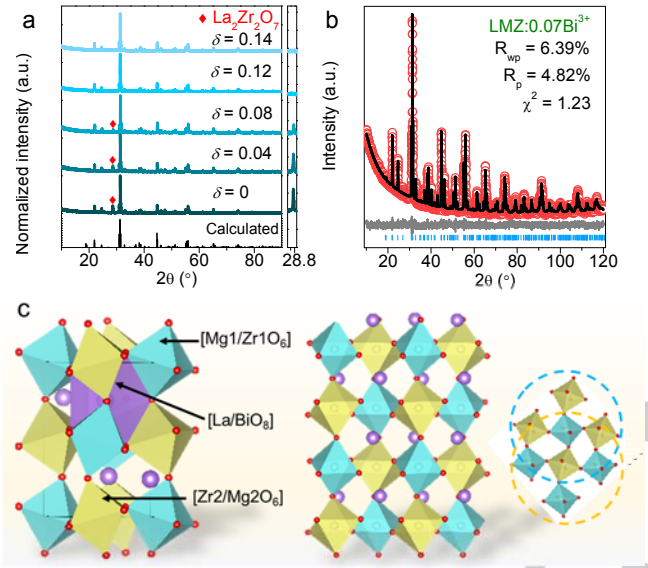

Figure 1. (a) XRD patterns of $LM_{(1+\delta)}Z_{(1-\delta)}$ ($0 \le \delta \le 0.14$) phosphors, calculated data of LMZ matrix and magnified XRD patterns from 28° to 29°, the red rhombus stands for impure $La_2Zr_2O_7$ phase. (b) Rietveld refinement of LMZ:0.07Bi^{3+} phosphor with the measured data (red circle), fitted data (black line), difference (grey line) and Bragg position (blue vertical bar). (c) The schematic crystal structure of LMZ matrix.

In Figure 1a, an impure $La_2Zr_2O_7$ phase (2θ = 28.67°) appears in La_2MgZrO_6:Bi^{3+} (δ = 0) phosphor. Then $La_2Zr_2O_7$ phase decreases and completely disappears with increasing Zr^{4+} stoichiometry at δ = 0.14 in $La_2Mg_{(1+\delta)}Zr_{(1-\delta)}O_6$:$Bi^{3+}$. All diffraction peaks of $La_2Mg_{1.14}Zr_{0.86}O_6$:$Bi^{3+}$ (LMZ:Bi^{3+}) match well with the calculated La_2MgZrO_6 matrix. Next, pure $La_2Mg_{1.14}Zr_{0.86}O_6$:*x*$Bi^{3+}$ ($0 \le x \le 0.1$) (LMZ:*x*Bi^{3+}) phosphors are successfully designed (Figure S1). To investigate the crystal structure of LMZ:*x*Bi^{3+}, Rietveld refinement was performed. The low *R*-factors confirm the formation of pure LMZ:*x*Bi^{3+} phases (Figure 1b and S2), and the main structure parameters of LMZ:0.07Bi^{3+} are collected in Table S1. The chemical formulas can be expressed as $La_2Mg_{1.13(4)}Zr_{0.87(4)}O_6$ and $La_2Mg_{1.12(4)}Zr_{0.88(4)}O_6$ for x = 0.03 and x = 0.07, respectively. These results are consistent with the designed $La_2Mg_{1.14}Zr_{0.86}O_6$ phase.

In Figure 1c, LMZ matrix exhibits a typical double perovskite structure ($A_2BB'O_6$) in a monoclinic structure ($P2_1/n$). LMZ matrix possesses one [LaO_8] polyhedron at A site and two types of [$Mg1/Zr1O_6$] and [$Zr2/Mg2O_6$] polyhedra at B and B' sites. Both B and B' sites are co-occupied by Mg^{2+} and Zr^{4+} ions. B sites are refined with linear restriction of $Occ_{Mg}(0.507)+Occ_{Zr}$ (0.493) = 1, and the occupancy of $Occ_{Mg}(0.401)+Occ_{Zr}(0.599)$ = 1 locates at B' site (Table S2). Moreover, every [Mg/ZrO_6] octahedron connects with four [Mg/ZrO_6] octahedra by vertex-sharing, constructing fundamental three-dimensional framework. La atom is coordinated by eight oxygen. Due to the similar ions radius between La^{3+} (CN = 8, r = 1.16 Å; CN represents coordination number, r is ions radius) and Bi^{3+}(CN = 8, r = 1.17 Å), Bi^{3+} ions are suggested to occupy La^{3+} sites. The lattice parameters (*a*, *c* and *V*) of LMZ:*x*Bi^{3+} linearly increase with increasing Bi^{3+} concentrations (Figure S3). The result confirms the successful substitution of the larger Bi^{3+} for La^{3+} ions. The slightly linear decrease of lattice parameter (*b*) might be ascribed to a lattice distortion. SEM images and corresponding elemental mapping data are exhibited in Figure S4. The representative LMZ:0.07Bi^{3+} phosphor presents irregular particles of 6-10 μm in diameter, and the smooth surface indicates a high crystallization. La, Zr, Mg, and Bi elements uniformly distribute in the whole visible area. These results also demonstrate the successful introduction of Bi^{3+} ions.

The UV-vis diffuse reflectance (DR) spectra of LMZ:*x*Bi^{3+} phosphors exhibit a broad absorption from 250 to 400 nm (Figure S5), which is assigned to $^1S_0\rightarrow{}^1P_1/{}^3P_1$ transition of Bi^{3+}. The optical bandgap of LMZ matrix equals to 5.34 eV, inferring that

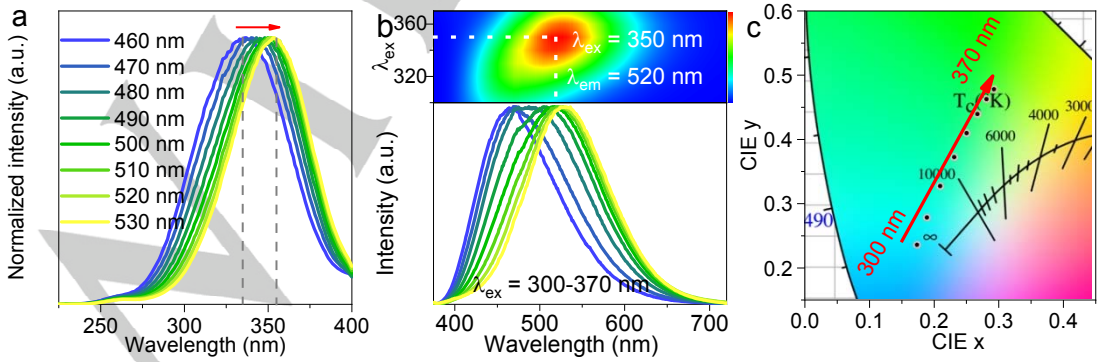

Figure 2. (a) Normalized PLE spectra (λ_{em} = 460-530 nm) of LMZ:0.07Bi^{3+} (b) The normal (top) and normalized (bottom) PL spectra of LMZ:0.07Bi^{3+} (λ_{ex} = 300-370 nm). (c) The CIE chromaticity coordinates diagram of LMZ:0.07Bi^{3+} under 300-370 nm excitation.

LMZ may act as a suitable phosphor matrix. The normalized photoluminescence excitation (PLE) spectra of LMZ:0.07Bi^{3+} agree well with the DR spectra results (Figure 2a), indicating the good accordance with n-UV LED chip. Interestingly, a small PLE redshift appears (325 → 350 nm) with varying emission wavelength (460-530 nm), of which the strongest excitation peak locates at 350 nm (Figure S6). Under 350 nm excitation, LMZ:*x*Bi^{3+} phosphors emit bright green light. The optimal Bi^{3+} concentration is 0.07 (Figure S7). This result indicates that LMZ:*x*Bi^{3+} phosphors have the potential application in LEDs lighting. Surprisingly, when changing the excitation wavelength from 300 to 370 nm with a step of 10 nm, the PL spectra of LMZ:0.07Bi^{3+} present consecutive redshift from 460 to 530 nm (Figure 2b). This excitation-induced PL redshift is rarely reported in Bi^{3+}-activated phosphors. In Figure 2b, the PL peak intensity changes with simultaneously changing excitation and emission wavelength, and the strongest PL peak locates at λ_{ex} = 350 nm and λ_{em} = 520 nm. The CIE coordination diagram intuitively presents a large photoluminescence tuning from blue (0.183, 0.236) to green (0.306, 0.487) by changing excitation wavelength (Figure 2c). Significantly, at other Bi^{3+} concentration, the similar PL redshift can also be observed by changing excitation or emission wavelength (Figure S8). This consequence excludes the influence of Bi^{3+} concentration on the PL redshift.

The PL decay curves of LMZ: 0.07Bi^{3+} are detected at λ_{ex} = 375 nm and λ_{em} =465-530 nm (Figure S9). The decay curves can be well fitted with the single exponential model, proving only one cation site for Bi^{3+} ions occupying. Moreover, the lifetime obviously increases from 448.8 ns (465 nm) to 613.1 ns (530 nm) (Table S3), directly confirming PL redshift. The above results imply that the continuous PL redshift does not come from multi-luminescence centers. Besides, under 350 nm excitation, no luminescence is observed in the LMZ matrix (Figure S10). These phenomena exclude the energy transfer from LMZ matrix to Bi^{3+} ions. The low-temperature PL spectra of LMZ:0.07Bi^{3+} at 7, 100 and 200 K also exhibit continuous PL redshift with excitation wavelength (Figure S11). The results are well consistent with the results at room temperature, and further excluding the influence of temperature on PL redshift. The above consequence indicates the stable excitation-induced PL redshift. According to the above investigations, other intrinsic factors should be responsible for the PL redshift in LMZ:*x*Bi^{3+} phosphors.

XPS spectra at Bi 4*f* of LMZ:0.05Bi^{3+}, LMZ:0.07Bi^{3+} phosphors and standard α-Bi_2O_3 are analyzed to identify the valence (Figure S12). Compared to the standard α-Bi_2O_3, the XPS signals of LMZ:0.05Bi^{3+}, LMZ:0.07Bi^{3+} phosphors slightly shift to low-energy side. Through Gaussian fitting analysis of LMZ:0.07Bi^{3+} phosphor (Figure 3a), two peaks (blue area) at 158.22 eV ($4f_{7/2}$) and 163.72 eV ($4f_{5/2}$) are assigned to Bi^{2+}, and the other two peaks (purple area) at 159.1 ($4f_{7/2}$) and 164.24 eV ($4f_{5/2}$) belong to Bi^{3+} [27]. Thus, Bi^{2+} and Bi^{3+} co-exist in LMZ:*x*Bi^{3+} phosphors, which might contribute to the abnormal PL redshift. Meanwhile, the XPS spectra at O 1*s* of LMZ matrix and LMZ:0.07Bi^{3+} can be fitted into four subpeaks (Figure 3b), two higher binding energy sides of O 1*s* (pink area) are attributed to the loosely bound oxygen. The two lower binding energy sides of O 1*s* (orange area) mean the presence of oxygen vacancies (*Vo*) [28]. These results demonstrate that *Vo* exists in both LMZ matrix and LMZ:0.07Bi^{3+} phosphor. In LMZ matrix, the cationic charge numbers are 11.72, which is smaller than the anionic charge numbers (12). Therefore, the obtained *Vo* is caused by the native defects, which has a significant effect on the generation of Bi^{2+}.

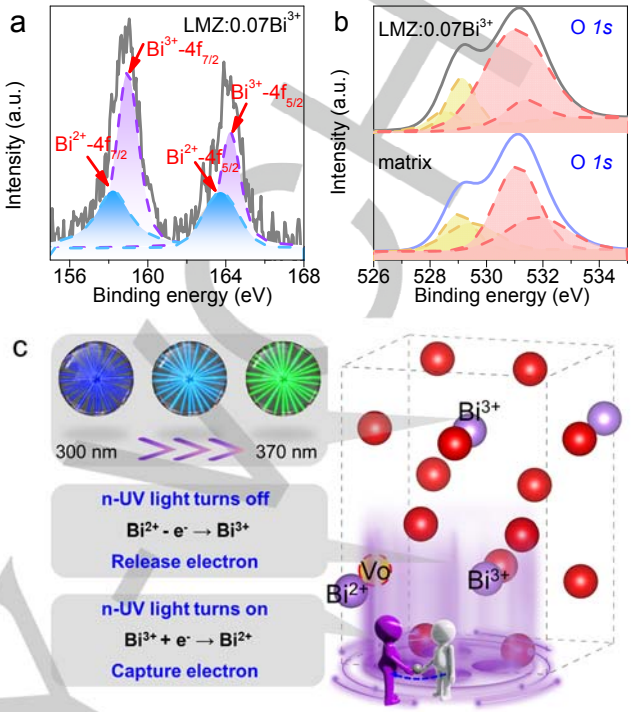

Figure 3. (a) Gaussian fitting peaks for XPS spectra of (a) Bi 4f and (b) O 1*s* for LMZ matrix and LMZ:0.07Bi^{3+} phosphors. (c) A schematic mechanism for excitation-induced PL redshift in LMZ:*x*Bi^{3+}.

As shown in Figure 3c, it infers that *Vo* randomly distributes in the LMZ matrix. When *Vo* appears surrounding [La/BiO_8] polyhedra, easily resulting in locally excessive positive charge. Bi^{3+} ions will capture electron from external radiation and transform to Bi^{2+}, keeping local charge balance. Hence, as the n-UV light working, external driving force may lead to local self-reduction from Bi^{3+} to Bi^{2+}. In this case, Bi^{3+} and Bi^{2+} will co-exist in LMZ matrix. The interaction between Bi^{3+} and Bi^{2+} ions occurs, generating continuous PLE/PL redshift. However, Bi^{2+} can't stably exist in LMZ matrix. When the n-UV light turns off, Bi^{2+} will return to Bi^{3+} by releasing electron, and thus the characteristic luminescence of Bi^{2+} cannot be observed. Figure S13 displays the temperature-dependent PL spectra of LMZ:0.07Bi^{3+} phosphor (λ_{ex} = 350 nm). At 150°C, the PL intensity maintains 61% of initial intensity at 25°C. The calculated activated energy ΔE with Arrhenius equation ($I_T/I_0 = [1+Aexp(-\Delta E/kT)]^{-1}$) equals to 0.25 eV. The increasing nonradiative transition energy is the primary reason for emission loss.

Based on the wide overlap between the PL spectra of LMZ:0.07Bi^{3+} and PLE spectra of LMZ:0.01Eu^{3+} (Figure S14), the energy transfer between Bi^{3+} and Eu^{3+} is designed to expect the full-spectrum photoluminescence control. Figure S15 indicates the phase purity of LMZ:0.07Bi^{3+}, *y*Eu^{3+} ($0 \le y \le 0.05$) phosphors. The photoluminescence properties, energy transfer efficiency (36%-70%) and the interaction relationship (dipole–dipole interaction) of Bi^{3+}→Eu^{3+} are discussed in details (Figure S16-S17), indicating that the photoluminescence color can be

controllably tuned by changing the excitation wavelength and Eu^{3+} concentration. Figure 4a and Table S4 exhibit the CIE coordinate positions of LMZ:0.07Bi^{3+}, *y*Eu^{3+} ($0 \le y \le 0.05$) phosphors. On the one hand, the photoluminescence color can be adjusted from blue/green to red light with increasing Eu^{3+} concentration (along x-axis direction). On the other hand, when fixing Eu^{3+} concentration, the photoluminescence color exhibits large shift with changing excitation wavelength (along y-axis direction). These results visibly reflect the wide two-dimensional color adjustment in the whole visible range. LMZ:0.07Bi^{3+}, 0.02Eu^{3+} even exhibits white light emission with varied CCT values, which is beneficial for the lighting application in multiple scenes. The representative digital photographs of LMZ:0.07Bi^{3+}, *y*Eu^{3+} ($0 \le y \le 0.05$) (λ_{ex} = 365 nm) are displayed in Figure 4b, all phosphors emit bright light. At suitable Eu^{3+} concentration and excitation wavelength, the phosphors can emit bright white light. Therefore, these phosphors can act as the potential single-composition white-emitting phosphors in LEDs applications. A conceptual LEDs device is presented in Figure 4c. The LEDs devices are constituted with LMZ:0.07Bi^{3+}, *y*Eu^{3+} ($0 \le y \le 0.05$) phosphors and wavelength-adjustable n-UV panel. When excitation light orderly passes wavelength collector (generate the excitation light), filter (select excitation wavelength), excitation controller (control the direction of the excitation light to reach a specific area), and finally reach at phosphors panel, the LEDs device will generate cyan (λ_{ex} = 310 nm) or green light (λ_{ex} = 350 nm). By precisely selecting Eu^{3+} concentration and excitation wavelength, the LEDs can emit the desired light based on the actual requirement. According to the precise photoluminescence color and CCT control, the conceptual LEDs can meet people's high-quality life demand.

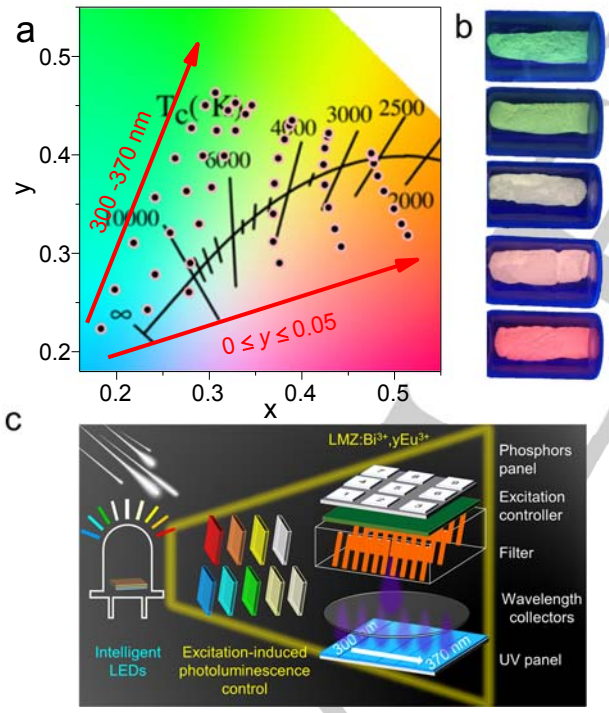

Figure 4. (a) The CIE chromaticity coordinates diagram for LMZ:0.07Bi^{3+}, *y*Eu^{3+} ($0 \le y \le 0.05$) phosphors. (b) The photoluminescence photographs of LMZ:0.07Bi^{3+}, *y*Eu^{3+} ($0 \le y \le 0.05$) under 365 nm irradiation. (c) The design concept of the intelligent LEDs devices.

In summary, an excitation-induced photoluminescence tuning is successfully achieved in LMZ:Bi^{3+} phosphors (PL peak shifts from 460 to 530 nm). Owing to the charge imbalance, oxygen vacancy stably exists in the LMZ matrix, which enables the self-reduction of Bi^{3+} to Bi^{2+} ions. The corresponding mechanism of the excitation-induced PL redshift is mainly ascribed to the coexistence of Bi^{3+} and Bi^{2+} ions. Through designing $Bi^{3+}\rightarrow Eu^{3+}$ energy transfer, a wide two-dimensional photoluminescence tuning is achieved by varying Eu^{3+} concentration and excitation wavelength. On the basis of the unique photoluminescence properties of LMZ:0.07Bi^{3+}, *y*Eu^{3+}, a conceptual LEDs device is designed, which can realize precise photoluminescence control with photoluminescence color and CCT. This work initiates a novel insight to design excitation-induced-photoluminescence-tunable phosphors for future intelligent LEDs lighting.

Experimental Section

The typical synthesis process and characterization are shown in the supporting information section.

Acknowledgments

This work was supported by the National Natural Science Foundation of China (Grant Nos. 51672259).

Keywords: intelligent LEDs • excitation-induced PL redshift • full-spectrum tuning • double perovskite structure

[1] X. Qin, X. Liu, W. Huang, M. Bettinelli, X. Liu, *Chem. Rev.* **2017**, *117*, 4488-4527.

[2] L. Wang, R. J. Xie, T. Suehiro, T. Takeda, N. Hirosaki, *Chem. Rev.* **2018**, *118*, 1951-2009.

[3] TrendForce 2020 Global LED Lighting Market Outlook- Light LED and LED Lighting Market Trend-1H20 (PDF) https://www.trendforce.com/research/download/RP200215XO

[4] Y. H. Kim, P. Arunkumar, B. Y. Kim, S. Unithrattil, E. Kim, S.-H. Moon, J. Y. Hyun, K. H. Kim, D. Lee, J.-S. Lee, W. B. Im, *Nat. Mater.* 2017, *16*, 543-550.

[5] J. Qiao, L. Ning, M. S. Molokeev, Y. C. Chuang, Q. Liu, Z. Xia, *J. Am. Chem. Soc.* **2018**, *140*, 9730-9736.

[6] Z. Tang, Q. Zhang, Y. Cao, Y. Li, Y. Wang, *Chem. Eng. J.* **2020**, *388*, 124231.

[7] Y. Wei, Z. Gao, S. Liu, S. Chen, G. Xing, W. Wang, P. Dang, A. A. Al Kheraif, G. Li, J. Lin, *Adv. Optical Mater.* **2020**, *8*, 1901859.

[8] Z. Wang, Q. Zhu, X. Wang, X. Li, X. Sun, B. N. Kim, J. G. Li, *Inorg. Chem.* **2019**, *58*, 890-899.

[9] W. Ji, S. Ye, M.-H. Lee, L. Hao, X. Xu, S. Agathopoulos, D. Zheng, C. Fang, Y. Huang, *J. Mater. Chem. C* **2016**, *4*, 3313-3320.

[10] G. J. Hoerder, S. Peschke, K. Wurst, M. Seibald, D. Baumann, I. Stoll, H. Huppertz, *Inorg. Chem.* **2019**, *58*, 12146-12151.

[11] W. B. Park, S. P. Singh, K. S. Sohn, *J. Am. Chem. Soc.* **2014**, *136*, 2363-2373.

[12] H. Chen, Y. Wang, *Inorg. Chem.* **2019**, *58*, 7440-7452.

[13] R. Shi, L. Ning, Z. Wang, J. Chen, T.-K. Sham, Y. Huang, Z. Qi, C. Li, Q. Tang, H. Liang, *Adv. Optical Mater.* **2019**, *7*, 1901187.

[14] M. Zhao, Z. Xia, M. S. Molokeev, L. Ning, Q. Liu, *Chem. Mater.* **2017**, *29*, 6552-6559.

[15] Z. Xia, G. Liu, J. Wen, Z. Mei, M. Balasubramanian, M. S. Molokeev, L. Peng, L. Gu, D. J. Miller, Q. Liu, K. R. Poeppelmeier, *J. Am. Chem. Soc.* **2016**, *138*, 1158-1161.

[16] X. Li, P. Li, Z. Wang, S. Liu, Q. Bao, X. Meng, K. Qiu, Y. Li, Z. Li, Z. Yang, *Chem. Mater.* **2017**, *29*, 8792-8803.

[17] M.-H. Fang, S. Mahlik, A. Lazarowska, M. Grinberg, M. S. Molokeev, H.-S. Sheu, J.-F. Lee, R.-S. Liu, *Angew. Chem. Int. Ed.* **2019**, *58*, 7767-7772.

[18] Y. Zheng, H. Zhang, H. Zhang, Z. Xia, Y. Liu, M. S. Molokeev, B. Lei, *J. Mater. Chem. C* **2018**, *6*, 4217-4224.

[19] F. Kang, H. Zhang, L. Wondraczek, X. Yang, Y. Zhang, D. Y. Lei, M. Peng, *Chem. Mater.* **2016**, *28*, 2692-2703.

[20] W. Zhou, Y. Ou, X. Li, M. G. Brik, A. M. Srivastava, Y. Tao, H. Liang, *Inorg. Chem.* **2018**, *57*, 14872-14881.

[21] Z. Gan;, H. Xu;, Y. Haoc, *Nanoscale* **2016**, *8*, 7794–7807.

[22] M. Xie, H. Wei, W. Wu, *Inorg. Chem.* **2019**, *58*, 1877-1885.

[23] Z. Tan, J. Li, C. Zhang, Z. Li, Q. Hu, Z. Xiao, T. Kamiya, H. Hosono, G. Niu, E. Lifshitz, Y. Cheng, J. Tang, *Adv. Funct. Mater.* **2018**, *28*, 1801131.

[24] J. Han, F. Pan, M. S. Molokeev, J. Dai, M. Peng, W. Zhou, J. Wang, *ACS Appl. Mater. Interfaces* **2018**, *10*, 13660-13668.

[25] J. Han, L. Li, M. Peng, B. Huang, F. Pan, F. Kang, L. Li, J. Wang, B. Lei, *Chem. Mater.* **2017**, *29*, 8412-8424.

[26] Q. Hu, G. Niu, Z. Zheng, S. Li, Y. Zhang, H. Song, T. Zhai, J. Tang, *Small*, **2019**, *15*, 1903496.

[27] X. Qin, Y. Li, D. Wu, Y. Wu, R. Chen, Z. Ma, S. Liu, J. Qiu, *RSC Adv.* **2015**, *5*, 101347-101352.

[28] Y. Wei, G. Xing, K. Liu, G. Li, P. Dang, S. Liang, M. Liu, Z. Cheng, D. Jin, J. Lin, *Light Sci. Appl.* **2019**, *8*,15.

Entry for the Table of Contents

COMMUNICATION

Wide photoluminescence tuning and varied-CCT white light by changing excitation wavelength and designing $Bi^{3+} \rightarrow Eu^{3+}$ energy transfer for future intelligent LEDs lighting.

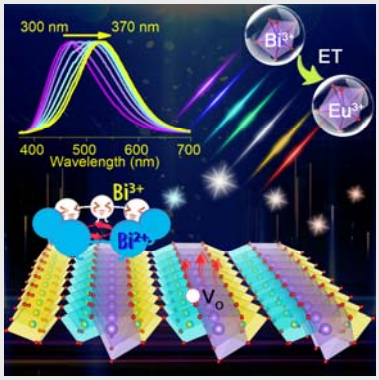

*Yi Wei, Hang Yang, Zhiyu Gao, Gongcheng Xing, Maxim S. Molokeev, Guogang Li**

Page No 1. – Page No. 5

Excitation and Valence Induced Photoluminescence Control in Bi-Eu Activated Double Perovskite Phosphor for Future Intelligent LEDs Lighting